# First-principles thermodynamics from phonon and Debye model: Application to Ni and Ni₃Al

Shun-Li Shang *, Yi Wang, DongEung Kim, Zi-Kui Liu

Department of Materials Science and Engineering, The Pennsylvania State University, University Park, PA 16802, USA

## ABSTRACT

Starting from first-principles projector-augmented wave method, finite temperature thermodynamic properties of Ni and Ni₃Al, including thermal expansion coefficient, bulk modulus, entropy, enthalpy and heat capacity, have been studied in terms of quasiharmonic approach. The thermal electronic contribution to Helmholtz free energy is estimated from the integration over the electronic density of state. The vibrational contribution to Helmholtz free energy is described by two methods: (i) the first-principles phonon via the supercell method and (ii) the Debye model with the Debye temperatures determined by Debye–Grüneisen approach and Debye–Wang approach. At 0 K, nine 4-parameter and 5-parameter equations of state (EOS's) are employed to fit the first-principles calculated static energy (without zero-point vibrational energy) vs. volume points, and it is found that the Birch-Murnaghan EOS gives a good account for both Ni and Ni₃Al among the 4-parameter EOS's, while the Murnaghan EOS and the logarithmic EOS are the worse ones. By comparing the experiments with respect to the ones from phonon, Debye–Grüneisen and Debye–Wang models, it is found that the thermodynamic properties of Ni and Ni₃Al studied herein (except for the bulk modulus) are depicted well by the phonon calculations, and also by the Debye models through choosing suitable parameters. The presently comparative studies of Ni and Ni₃Al by phonon and Debye models, as well as by different EOS's, provide helpful insights into the study of thermodynamics for solid phases at elevated temperatures.

© 2009 Elsevier B.V. All rights reserved.

## 1. Introduction

The parameter-free first-principle calculations, e.g. based on the density functional theory, require only knowledge of the atomic species and crystal structure, and hence, are predictive in nature. In combination with quasiharmonic approach, finite temperature thermodynamics of sold phase can be depicted accurately in terms of first-principles calculations (see examples in [1–8]), wherein the used Helmholtz free energy $F(V, T)$ at volume $V$ and temperature $T$ is usually approximated by,

$$F(V, T) = E(V) + F_{el}(V, T) + F_{vib}(V, T) \quad (1)$$

where $E(V)$ is the static energy (without zero-point vibrational energy) at 0 K and volume $V$ predicted by e.g. first-principles calculations, and fitted by an equation of state (EOS). $F_{el}(V, T)$ represents the thermal electronic contribution to free energy with respect to the corresponding $V$ and $T$, which is in particular important for metal (instead of semiconductor and insulator) system due to the non-zero electronic density at the Fermi level. $F_{vib}(V, T)$ is the vibrational contribution to free energy, usually described by phonon calcula-

tions for the sake of accuracy [1,3,8] or by Debye model for the sake of simplicity and efficiency [4,6,7]. Although there exist comparative researches of pressure vs. volume (P–V) EOS's at high pressures (see e.g. [9]), few attentions have been paid to the fittings of different E–V EOS's. Furthermore, comparative researches of vibrational contributions from phonon and Debye models are also scarce in the literature (see [10] for the study of MgSiO₃). The dearth of the aforementioned studies therefore motivates this work.

In the present work, first-principles thermodynamics of Ni with fcc structure and Ni₃Al with L1₂ structure will be studied based on Eq. (1), aiming to evaluate the fittings of different EOS's and the vibrational contributions obtained from phonon and Debye models. The selections of Ni and Ni₃Al are due to the technologically important Ni-based superalloy, and in particular the newly developed coatings by Gleeson and co-workers [11,12] have demonstrated oxidation kinetics a factor of 10–20 slower than the current Pt-modified NiAl coatings. These new coatings are based on the two-phase mixture of Ni + Ni₃Al in the Ni–Al–Pt system and further modified with Cr, Hf, Y and Zr, with Ni₃Al being the major phase. Since these new coatings have the same constitution as Ni-based superalloys, they have opened the path to the development of highly oxidation resistant and compatible coatings for current and future generation of superalloys. Based on first-principles

phonon calculations, Wang et al. [1] described the thermodynamic properties of Ni and Ni$_3$Al by the linear response theory [13], and later on Arroyave et al. [2] described them by the supercell method [14], wherein the thermal electronic contributions were included and discussed in both works. The studies of EOS's and Debye model were not mentioned in [1,2], while they will be the main topics of this work.

In the present work, we organize the paper as follows. In Section 2, we present firstly the widely used 4-parameter and 5-parameter EOS's, and then the theories to calculate the thermal electronic contribution from electronic density of state (DOS) and the vibrational contribution based on phonon DOS and Debye models. In Section 3, details of electronic structures and first-principles phonon results are presented. Herein the first-principles calculations are performed by VASP code [15,16]; the phonon calculations are carried out by the supercell approach [14] as implemented in ATAT code [17]. In Section 4, we discuss the EOS fittings and the first-principles thermodynamics for Ni and Ni$_3$Al. Finally, in Section 5 the conclusions of the present work are given.

## 2. Theory

In order to describe the first-principles thermodynamics using Eq. (1), details of the equations and methods will be presented in this Section including the energy vs. volume ($E$–$V$) EOS's (Section 2.1), the thermal electronic contribution to Helmholtz free energy (Section 2.2), and the vibrational contribution to Helmholtz free energy by phonon and two Debye models (Section 2.3).

### 2.1. Energy vs. volume equations of state

A lot of $E$–$V$ and correspondingly the $P$–$V$ EOS's are presented in the literature, and each of them possesses its application for some materials. Therefore, we need to choose a suitable EOS, based on such as the minimum fitting errors as described below. The available $E$–$V$ EOS's can be grouped into linear and non-linear ones, where the linear ones can be written in matrix form enabling the fit parameters to be solved by (pseudo-)inversion, and the matrix form is easily implemented in e.g. the cluster expansion method [7]. Therefore the linear EOS's will be the first choice if possible. The widely used linear EOS's are the Birch-Murnaghan (BM) EOS [18,19] and the modified one (mBM EOS) [7,20]. Their 5-parameter equation has the following common format:

$$E(V) = a + bV^{-n/3} + cV^{-2n/3} + dV^{-3n/3} + eV^{-4n/3} \tag{2}$$

where $a$, $b$, $c$, $d$, and $e$ are the fitting parameters, for 4-parameter cases $e = 0$. When $n = 2$, it is the BM EOS; when $n = 1$, Eq. (2) becomes the mBM EOS proposed by Teter et al. [20]. Another commonly used linear EOS is the logarithmic (LOG) one [21],

$$E(V) = a + b \ln V + c(\ln V)^2 + d(\ln V)^3 + e(\ln V)^4 \tag{3}$$

where $a$, $b$, $c$, $d$, and $e$ are also the fitting parameters with $e = 0$ for 4-parameter case. The LOG EOS is believed to offer better performance at high pressures than the BM EOS.

Besides the linear EOS's in the forms of Eqs. (2) and (3), the non-linear EOS's studied in the present work are Murnaghan [22], Vinet [23,24] and Morse [5] EOS's. The 4-parameter Murnaghan EOS [22] has the following form:

$$E(V) = a + \frac{B_0 V}{B_0'} \left( 1 + \frac{(V_0/V)^{B_0'}}{B_0' - 1} \right) \tag{4}$$

where the fitting parameter $a = E_0 - \frac{B_0 V_0}{B_0' - 1}$. The parameters $V_0$, $E_0$, $B_0$, and $B_0'$ represent the equilibrium volume, energy, bulk modulus,

and its first derivate with respect to pressure, respectively. The non-linear 4-parameter Vinet EOS [23,24] is in the form of,

$$E(V) = a - \frac{4B_0 V_0}{(B_0' - 1)^2} \left\{ 1 - \frac{3}{2}(B_0' - 1)\left[ 1 - \left(\frac{V}{V_0}\right)^{1/3} \right] \right\}$$
$$\times \exp\left\{ \frac{3}{2}(B_0' - 1)\left[ 1 - \left(\frac{V}{V_0}\right)^{1/3} \right] \right\} \tag{5}$$

where the fitting parameter $a = E_0 + \frac{4B_0 V_0}{(B_0' - 1)^2}$. Additionally, the 4-parameter non-linear Morse EOS [5] can be expressed by,

$$E(V) = a + b \exp(dV^{1/3}) + c \exp(2dV^{1/3}) \tag{6}$$

where $a$, $b$, $c$, and $d$ are the fitting parameters.

Starting from the $E$–$V$ EOS's, the volume-dependent pressure $P$, bulk modulus $B$, the first and the second derivates of bulk modulus with respect to pressure, $B'$ and $B''$, respectively, are obtained via,

$$P(V) = -V \frac{\partial E}{\partial V} \tag{7}$$

$$B(V) = V \frac{\partial^2 E}{\partial V^2} \tag{8}$$

$$B'(V) = \frac{\partial B}{\partial P} = \frac{\partial B}{\partial V} \bigg/ \frac{\partial P}{\partial V} \tag{9}$$

$$B''(V) = \frac{\partial^2 B}{\partial P^2} = \left( \frac{\partial^2 B}{\partial V^2} \frac{\partial P}{\partial V} - \frac{\partial^2 P}{\partial V^2} \frac{\partial B}{\partial V} \right) \bigg/ \left( \frac{\partial P}{\partial V} \right)^3 \tag{10}$$

As an example, for BM4 EOS (Eq. (2) with $n = 2$ and $e = 0$), the determinations of equilibrium properties $V_0$, $B_0$, and $B_0'$ are given in Appendix A. For another example of mBM4 EOS (Eq. (2) with $n = 1$ and $e = 0$), the formulae to estimate $V_0$, $B_0$, and $B_0'$ can be found in [7]. It is worth mentioning that $B''$ is a property obtained from 5-parameter EOS's, for 4-parameter cases $B''$ can be calculated from $B$ and $B'$ with details shown in Table 1. As listed in Table 1, $B'' = 0$ holds for Murnaghan EOS.

Inversely, starting from the equilibrium properties $E_0$, $V_0$, $B_0$, $B_0'$, and $B_0''$, the EOS's can be obtained directly, just like the cases of Murnaghan EOS shown in Eq. (4) and Vinet EOS shown in Eq. (5). In Table A1 of Appendix A, the equations of fitting parameters represented by equilibrium properties are shown for BM, mBM, LOG and Morse EOS's.

Furthermore, according to the first-principles practices of EOS fitting, the EOS should be performed in a single phase region, and in general the first-principles data points should be in the volume range of ±10% around the equilibrium volume, and at least five data points (>10 is better) should be employed. For magnetic materials (such as the Ni$_3$Al case below), care should be taken for the correspondingly magnetic moment vs. volume (MM-V) relationship: a sudden jump of MM-V usually indicates a signal of magnetic phase transition.

**Table 1**
Equilibrium property $B_0''$ in the 4-parameter EOS's represented by $B_0$ and $B_0'$.

| EOS | $B_0''$ |
|---|---|
| BM4 | $(-143 + 63B_0' - 9B_0'^2)/(9B_0)$ |
| mBM4 | $(-74 + 45B_0' - 9B_0'^2)/(9B_0)$ |
| LOG4 | $(-3 + 3B_0' - B_0'^2)/B_0$ |
| Murnaghan | 0 |
| Vinet | $(19 - 18B_0' - 9B_0'^2)/(36B_0)$ |
| Morse | $(5 - 5B_0' - 2B_0'^2)/(9B_0)$ |

## 2.2. Thermal electronic contribution to Helmholtz free energy

Thermal electronic contribution to Helmholtz free energy is determined by Mermin statistics $F_{el} = E_{el} - TS_{el}$, where the internal energy at the volume $V$ and temperature $T$ due to electronic excitations is given by [1],

$$E_{el}(V,T) = \int n(\varepsilon) f \varepsilon d\varepsilon - \int^{\varepsilon_F} n(\varepsilon) \varepsilon d\varepsilon \qquad (11)$$

where $n(\varepsilon)$ is the electronic DOS, $\varepsilon$ the energy eigenvalues, $\varepsilon_F$ the energy at the Fermi level, $f$ the Fermi distribution function $f(\varepsilon, T, V) = 1/\{\exp(\frac{\varepsilon - \mu(T,V)}{k_B T}) + 1\}$ with $k_B$ the Boltzmann's constant and $\mu$ the electronic chemical potential which should be carefully calculated to keep the number of electrons at $T$ to be constant (the same as the number at 0 K and below $\varepsilon_F$). The bare electronic entropy due to electronic excitations is written by [1],

$$S_{el}(V,T) = -k_B \int n(\varepsilon)[f \ln f + (1-f) \ln(1-f)] d\varepsilon \qquad (12)$$

Note that the thermal electronic contribution is usually for metal only (instead of semiconductor and insulator), the shape and DOS around the Fermi level determine mainly the thermal electronic contributions to Helmholtz free energy.

## 2.3. Vibrational contributions to Helmholtz free energy

### 2.3.1. Vibrational contribution from phonon
Based on the distribution of frequency $\omega$, i.e. the phonon DOS $g(\omega)$, at a given volume $V$, vibrational contribution to Helmholtz free energy can be written as follows according to the partition function of lattice vibration (see e.g. [1,8]),

$$F_{vib}(V,T) = k_B T \int_0^\infty \ln\left[2 \sinh \frac{\hbar\omega}{2k_B T}\right] g(\omega) d\omega, \qquad (13)$$

where $\hbar$ is the reduced Planck constant. Based on phonon DOS, the $n$th moment Debye cutoff frequency and the corresponding $n$th moment Debye temperature can be determined, where the Debye cutoff frequencies are given by [25],

$$\omega_n = \left[\frac{n+3}{3} \int_0^{\omega_{\max}} \omega^n g(\omega) d\omega\right]^{1/n}, \quad \text{with } n \neq 0, n > -3 \qquad (14)$$

$$\omega_0 = \exp\left[\frac{1}{3} + \int_0^\infty \omega^n \ln(\omega) d\omega\right], \quad \text{with } n = 0 \qquad (15)$$

Thus, the $n$th moment Debye temperature is obtained by,

$$\Theta_D(n) = \frac{\hbar}{k_B} \omega_n \qquad (16)$$

With different value of $n$, the obtained Debye temperature corresponds to different meanings [3], for example, $\Theta_D(2)$ usually links to the Debye temperature obtained from the heat capacity data, and will be used in the present work.

### 2.3.2. Vibrational contribution from Debye model
For the sake of simplicity or many structures needed to be treated, the vibrational contribution to Helmholtz free energy can be estimated by the empirical Debye model (see e.g. [26]),

$$F_{vib}(V,T) = \frac{9}{8} k_B \Theta_D + k_B T \left\{3 \ln\left[1 - \exp\left(-\frac{\Theta_D}{T}\right)\right] - D\left(\frac{\Theta_D}{T}\right)\right\} \qquad (17)$$

where $D(\Theta_D/T)$ is the Debye function given by $D(x) = 3/x^3 \int_0^x t^3/[\exp(t) - 1] dt$. In order to evaluate Eq. (17), the key is to obtain the Debye temperature $\Theta_D$. In terms of Debye–Grüneisen model [5], $\Theta_D$ is written by,

$$\Theta_D = sAV_0^{1/6}\left(\frac{B_0}{M}\right)^{1/2}\left(\frac{V_0}{V}\right)^\gamma \qquad (18)$$

where $s$ is a scaling factor with $s = 0.617$ obtained by Moruzzi et al. [5] from nonmagnetic cubic metals. Other $s$ values are also reported in the literature, e.g. $s = 0.7638$ for pure iron [27]. $M$ is the atomic mass, $\gamma$ is the Grüneisen constant defined by $\gamma = [(1 + B_0')/2 - x]$ with $x = 2/3$ for high temperature case and $x = 1$ for low temperature case [5]. The parameter $A$ is a constant with $A = (6\pi^2)^{1/3}\hbar/k_B = 231.04$ if $V$ in $\text{Å}^3$, $B$ (and $P$) in GPa, and $M$ in atomic mass of gram. Note that the Debye–Grüneisen model implicates that the Grüneisen constant is always a constant [5].

Without using the Grüneisen constant, Wang et al. [28] proposed a method to calculate the Debye temperature,

$$\Theta_D = sAV^{1/6}\left\{\frac{1}{M}\left[B - \frac{2(\lambda+1)}{3}P\right]\right\}^{1/2} \qquad (19)$$

where the parameter $\lambda$ in Debye–Wang model is adjustable with values commonly taken 0, ±1/2, and ±1. For instance, if $\lambda = -1$, Eq. (19) will be used in high temperature case; if $\lambda = 1$, Eq. (19) will be used in low temperature case (see [28] for details). The Debye–Wang model has been used further by Lu et al. [29,30]. It should be mentioned that both Eq. (18) and Eq. (19) will predict the same Debye temperature under equilibrium conditions with $V = V_0$, $B = B_0$, and $P = 0$.

## 3. Details of first-principles and phonon calculations

In the present work the first-principles calculations of Ni and Ni₃Al are performed by VASP code [15,16]. The electron–ion interactions are described by the full potential frozen-core PAW method [31,32], and the exchange–correlation is treated within the GGA of Perdew–Burke–Ernzerhof (PBE) [33]. The reason to choose the PAW method instead of the ultrasoft pseudo-potentials is that the PAW method combines the accuracy of all-electron methods with the efficiency of pseudo-potentials [32], as demonstrated in e.g. [34]. In VASP calculations, the wave functions are sampled on $22 \times 22 \times 22$ $k$-point mesh for Ni and $20 \times 20 \times 20$ for Ni₃Al based on Monkhorst–Pack scheme [35] together with the linear tetrahedron method including Blöchl corrections [36]. The energy cutoff on the wave function is taken as 350 eV, which is 1.3 times higher than the default values. The energy convergence criterion for electronic self-consistency is $10^{-7}$ eV per atom. Due to the ferromagnetic nature of Ni-containing materials, all the calculations are performed within the spin-polarized approximation.

The phonon calculations are carried out by the supercell method [14] as implemented in ATAT code [17], with VASP again the computational engine. We use the 72-atom and 48-atom supercells for Ni and Ni₃Al, respectively. Displacements of 0.1 Å are adopted in the perturbed supercells, resulting in the maximum force acting on atom is ~0.8 eV/Å at the equilibrium volume. In VASP calculations, we use the $4 \times 4 \times 4$ Monkhorst–Pack $k$-point mesh [35] and the Methfessel–Paxton technique [37]. After VASP calculations, the cutoff range of 6 Å is used to fit the force constants and to get the phonon results by ATAT. Additional details of phonon methodology can be found in [8].

## 4. Results and discussion

In this Section, we present the comparative studies of EOS's of Ni and Ni₃Al (Section 4.1), the electronic and phonon results of Ni and Ni₃Al (Section 4.2), and the vibrational contribution to Helmholtz free energy from phonon, Debye–Grüneisen and Debye–Wang models (Section 4.3). Note that we ignore herein the singular behaviors of thermodynamics (see the case of Ni below)

due to the magnetic phase transition from ferromagnetic phase to paramagnetic phase. On the other hand, the thermodynamics of Ni and Ni-containing materials possesses the similar behavior in the ferromagnetic and paramagnetic regions due to the small magnetic moment of Ni ($<1\mu_B$/atom, see below).

### 4.1. Properties from equations of state

VASP calculated static energies and magnetic moments of Ni and Ni$_3$Al are shown in Fig. 1 as a function of volume, together with the fittings by nine EOS's given in Eqs. (2)–(6). At lower volumes (e.g. <40 Å$^3$ per unit cell), the calculated Ni$_3$Al points are not shown in Fig. 1 due to the fact that Ni$_3$Al is convergent to nonmagnetic state. Table 2 shows the EOS's fitted equilibrium properties including volume $V_0$ (represented by lattice parameter), bulk modulus $B_0$ and its first and second derivates with respect to pressure: $B_0'$ and $B_0''$, respectively, together with the fitting error estimated by,

$$\sqrt{\frac{\sum[(E_{fit} - E_{calc})/E_{calc}]^2}{k}} \tag{20}$$

where $E_{fit}$ and $E_{calc}$ are the fitted and the first-principles calculated energies, respectively, $k$ represents the total number of the calculated points. As shown in Fig. 1 and Table 2, the 5-parameter EOS's (mBM5, BM5 and LOG5) give better fittings of $E$–$V$ points than the 4-parameter ones. Among the 4-parameter EOS's, the BM4 is the best one with the smallest fitting errors for both Ni and Ni$_3$Al (see Table 2), while the LOG4 and the Murnaghan are the worse ones due to that $B'' = 0$ will be predicted by Murnaghan EOS (see Table 1), and the logarithmic ones (LOG4 and LOG5, see Eq. (3)) cannot

**Table 2**
Fitted properties by EOS's together with the measurements, including lattice parameter $a_0$ (Å), bulk modulus $B_0$ (GPa) and its first and second derivates with respect to pressure, $B_0'$ and $B_0''$ (1/GPa), respectively. The fitting errors estimated by Eq. (20) are also shown.

| Material | Method | $a_0$ | $B_0$ | $B_0'$ | $B_0''$ | Error ($\times 10^{-4}$) |
|---|---|---|---|---|---|---|
| Ni | mBM4 | 3.5231 | 196.5 | 4.98 | −0.0414 | 1.427 |
| | mBM5 | 3.5235 | 194.0 | 4.96 | −0.0329 | 0.078 |
| | BM4 | 3.5237 | 193.1 | 4.94 | −0.0295 | 0.540 |
| | BM5 | 3.5235 | 193.9 | 4.96 | −0.0328 | 0.081 |
| | LOG4 | 3.5224 | 204.0 | 4.98 | −0.0631 | 5.626 |
| | LOG5 | 3.5232 | 193.9 | 5.03 | −0.0339 | 0.326 |
| | Murnaghan | 3.5258 | 185.6 | 4.73 | 0 | 4.952 |
| | Vinet | 3.5229 | 196.6 | 5.01 | −0.0420 | 1.491 |
| | Morse | 3.5231 | 195.9 | 5.00 | −0.0397 | 1.116 |
| | Expt. | 3.53[a] | 188[b] | | | |
| Ni$_3$Al | mBM4 | 3.5693 | 179.7 | 4.60 | −0.035 | 0.131 |
| | mBM5 | 3.5691 | 180.0 | 4.69 | −0.032 | 0.043 |
| | BM4 | 3.5690 | 180.1 | 4.74 | −0.029 | 0.085 |
| | BM5 | 3.5691 | 180.0 | 4.68 | −0.032 | 0.043 |
| | LOG4 | 3.5699 | 178.7 | 4.27 | −0.047 | 0.583 |
| | LOG5 | 3.5692 | 180.1 | 4.67 | −0.035 | 0.048 |
| | Murnaghan | 3.5679 | 181.0 | 5.27 | 0 | 0.807 |
| | Vinet | 3.5694 | 179.7 | 4.55 | −0.039 | 0.190 |
| | Morse | 3.5693 | 179.8 | 4.58 | −0.037 | 0.148 |
| | Expt. | 3.57[a] | 172[c] | | | |

[a] Estimated value based on measurements at room temperature [38].
[b] Recommended value at 0 K [39].
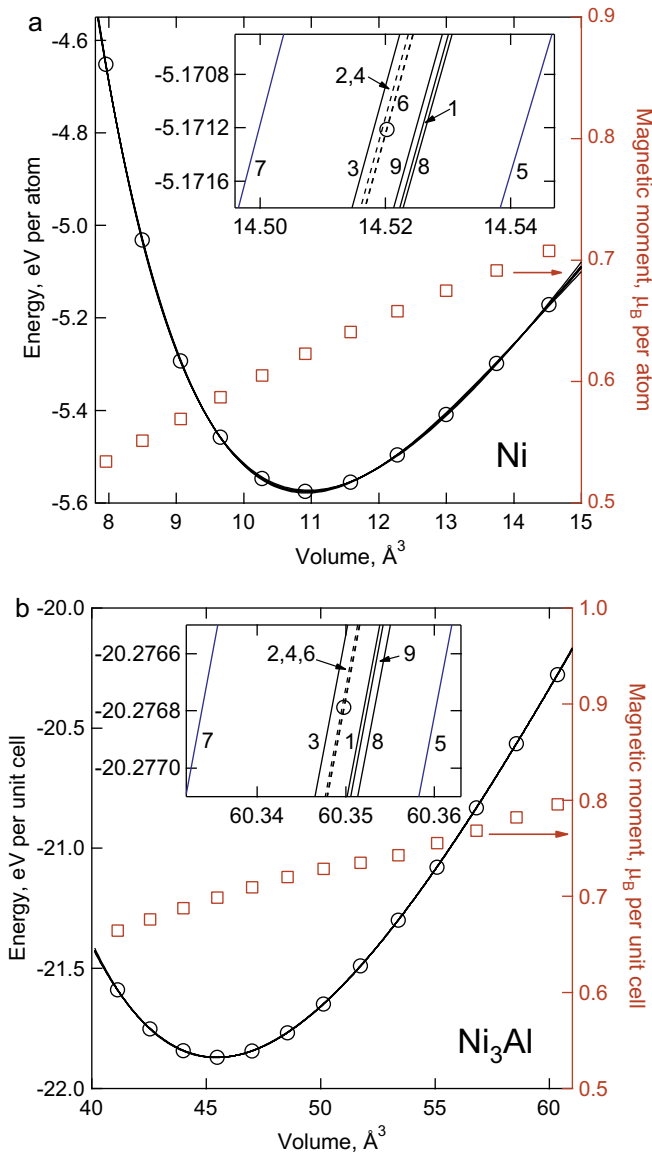[c] Measurement at room temperature [40].



**Fig. 1.** Calculated total energies (open cycles) and magnetic moments (open squares) for Ni and Ni$_3$Al as a function of volume, together with the fittings by nine EOS's given in Eqs. (2)–(6) with 1 – mBM4 (4-parameter EOS), 2 – mBM5 (5-parameter EOS), 3 – BM4, 4 – BM5, 5 – LOG4, 6 – LOG5, 7 – Murnaghan, 8 – Vinet, and 9 – Morse. The 5 - parameter EOS's (2), (4), and (6) are shown in dashed lines, the 4-parameter ones are shown in solid lines.
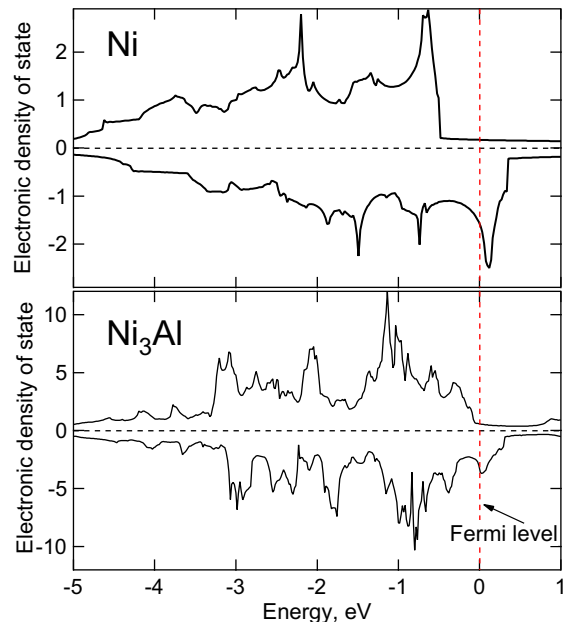


**Fig. 2.** Calculated electronic densities of state around Fermi level for Ni and Ni$_3$Al.

predict $E \propto 0$ when $V \propto (+\infty)$. As for the 5-parameter EOS's, bad fittings will be resulted when the $E$-$V$ points are scattered. Therefore, the 4-parameter EOS's are recommended. In the present work, the BM4 (Eq. (2) with $n = 2$ and $e = 0$) is used as it possesses the smallest fitting error.

Table 2 also shows that the fitted lattice parameters of Ni and Ni₃Al by different EOS's are close to each other, and agree with measurements at room temperature [38]. For Ni, the maximum bulk modulus of 204 GPa is fitted by LOG4, while the minimum one of 186 GPa is given by Murnaghan EOS. By considering the less accurate fittings of LOG4 and Murnaghan, the fitted bulk modulus of Ni should be around 193–196 GPa, which is slightly larger than the measured 188 GPa at 0 K [39]. For Ni₃Al, the fitted bulk modulus is around 180 GPa (without considering the results from LOG4 and Murnaghan, also true for the rest discussions), which is 3% larger than the measured ~172 GPa at room temperature [40]. Regarding $B_0'$, the EOS's predict ~5 for Ni and ~4.7 for Ni₃Al. For $B_0''$, the 5-parameter EOS's give values around −0.033 GPa⁻¹ for Ni and −0.035 GPa⁻¹ for Ni₃Al. $B_0''$'s in the 4-parameter EOS's, which are obtained from $B$ and $B_0'$, are also shown in Table 1. The close values of $B_0''$ between the 5-parameter and the 4-parameter EOS's indicate the fittings are in good quality. In addition, Table 2 also shows that the fitting qualities of Ni₃Al are in general better than those of Ni as indicated by the fitting errors.

## 4.2. Electronic and phonon properties

First-principles calculated electronic DOS's of Ni and Ni₃Al at the theoretical equilibrium volumes (see Table 2) are shown in

Fig. 2. For both materials, the Fermi levels locate in the dip places, indicating the stabilities of ferromagnetic phases of fcc Ni and L1₂ Ni₃Al. In addition, the non-zero densities around the Fermi levels occur for Ni and Ni₃Al, implying the thermal electronic contribution to free energy should be considered, especially at high temperatures. For example of Ni, Wang et al. [1] indicate that more than 10% thermal electronic contribution to free energy (and other properties) happens for Ni if $T > 900$ K. Additionally, the including of thermal electronic contributions improves the agreements between the predicted thermodynamic properties and the measurements for both Ni and Ni₃Al [1,2]. Therefore, the thermal electronic contributions will be included (but without discussion) in the present work.

In order to verify the qualities of first-principles phonon calculations, Fig. 3 shows the predicted phonon dispersion curves at the theoretical equilibrium volumes (see Table 2) together with the room temperature measurements by neutron diffractions of Ni [25] and Ni₃Al [41]. A good agreement is observed between calculations and measurements, in particular for Ni. Based on the phonon results, the Debye temperatures can be estimated by Eq. (16). Herein the predicted second moment Debye temperatures
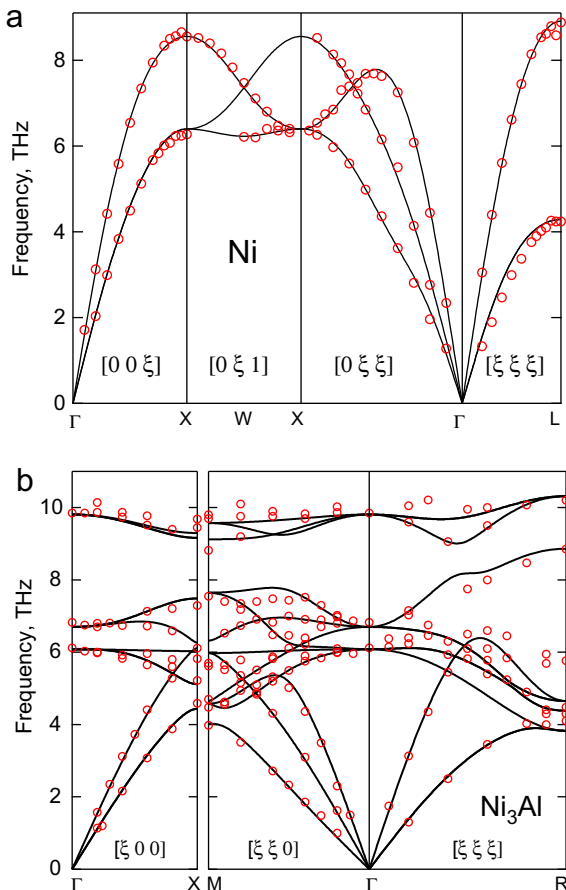


Fig. 3. Calculated phonon dispersion curves for Ni and Ni₃Al at the theoretical equilibrium volumes, together with the room measurements (symbols) of Ni [25] and Ni₃Al [41].
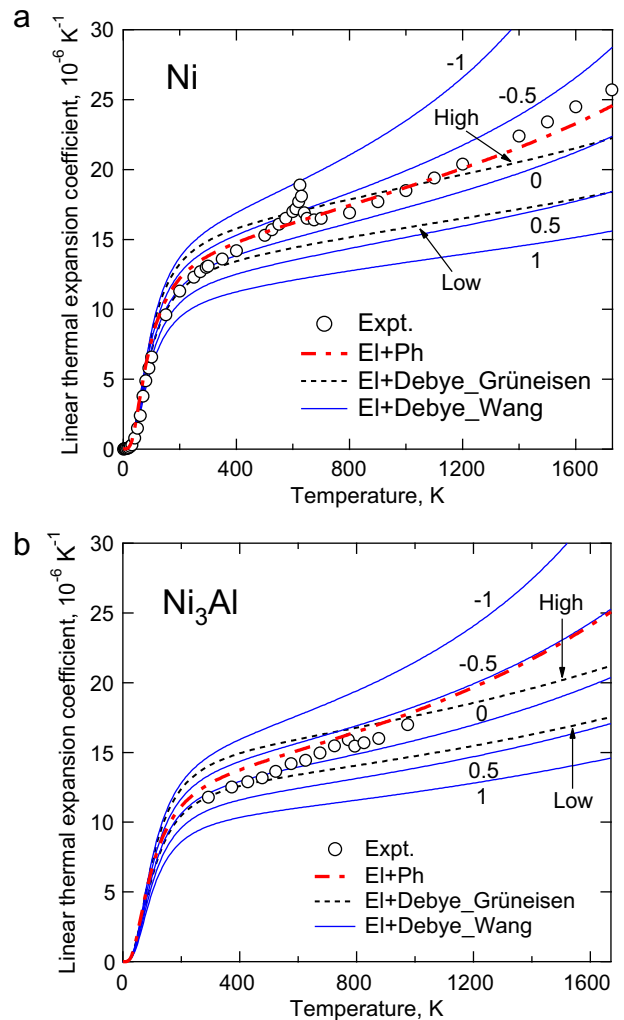


Fig. 4. Linear thermal expansion coefficients for Ni and Ni₃Al as a function of temperature calculated by (i) phonon plus thermal electronic contribution, (ii) Debye–Grüneisen model (high temperature and low temperature cases) plus thermal electronic contribution, and (iii) Debye–Wang model ($\lambda = 0$, ±0.5, and ±1) plus thermal electronic contribution. The recommended values (open cycles) are also shown for Ni [42] and Ni₃Al [43].

at the theoretical equilibrium volumes are 385 K and 425 K for Ni and Ni$_3$Al, respectively, agreeing well with the measured high temperature limits of ∼390 K [25] and ∼425 K [41]. The predicted Debye temperatures from phonon are used to adjust the scaling factors in both the Debye–Grüneisen model of Eq. (18) and the Debye–Wang model of Eq. (19), with the values of 0.617 and 0.65 obtained for Ni and Ni$_3$Al, respectively. It worth mentioning that the scaling factor is less important in Debye model, in comparison with the Grüneisen constant in Eq. (18) and the value of $\lambda$ in Eq. (19), therefore the later two will be discussed in Section 4.3.

### 4.3. Thermodynamic properties

The linear thermal expansion coefficient $\alpha$ at fixed pressure $P$ ($P = 0$ will be used in the present work) can be determined by,

$$\alpha = \frac{1}{3V_{0T}}\left(\frac{\partial V_{0T}}{\partial T}\right)_p \qquad (21)$$

where $V_{0T}$ is the equilibrium volume at the temperature of interest, determined by Eq. (1) at $P = 0$. Fig. 4 shows the linear thermal expansion coefficients of Ni and Ni$_3$Al, predicted by phonon, Debye–Grüneisen and Debye–Wang models. Note that the thermal

electronic contributions are included for all the thermodynamic properties discussed in this Section. The thermal expansion coefficients predicted by phonon agree well with the recommended values of Ni [42] and Ni$_3$Al [43]. As for the Debye model, the predicted thermal expansion coefficients depend heavily on the selected Grüneisen constant in Debye–Grüneisen model and the $\lambda$ value in Debye–Wang model. A large Grüneisen constant (i.e. the high temperature case, see Eq. (18)) and a small $\lambda$ value predict large thermal expansion coefficients at temperatures >100 K. A suitable selection of Grüneisen constant or $\lambda$ value will describe well the linear thermal expansion coefficients. In the present work, the high temperature case of Grüneisen constant in Debye–Grüneisen model and $\lambda = -0.5$ in Debye–Wang model predict results close to phonon and experiments for both Ni and Ni$_3$Al.

Fig. 5 shows the temperature-dependent bulk moduli of Ni and Ni$_3$Al obtained by phonon, Debye–Grüneisen model, Debye–Wang model, together with the available measurements [39,40]. For both Ni and Ni$_3$Al, the measured bulk moduli are in general higher than most of the predictions, agreeing with the low temperature case of Debye–Grüneisen model and $\lambda = 1$ of Debye–Wang model, instead of phonon predictions.
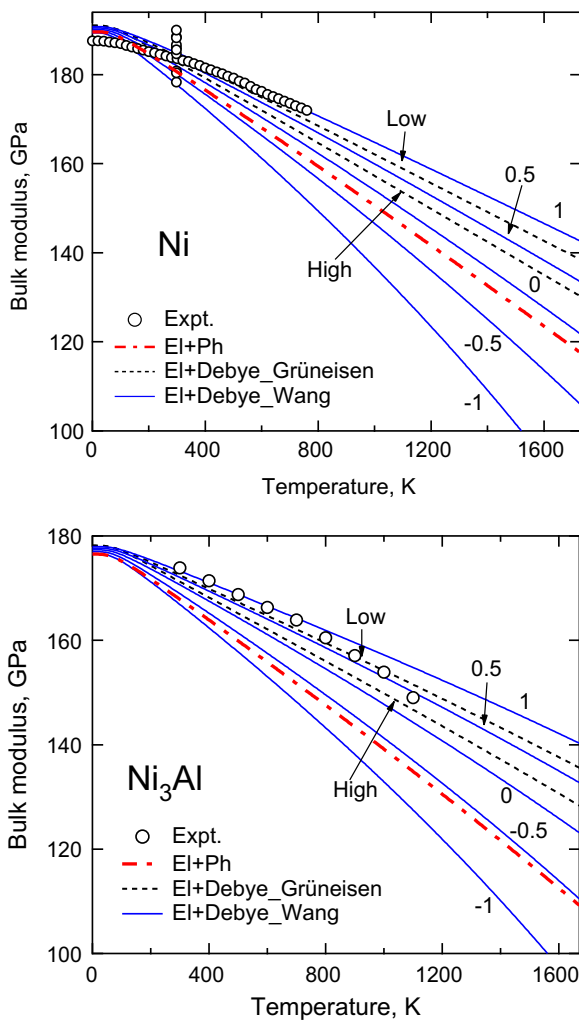


Fig. 5. Bulk moduli for Ni and Ni$_3$Al as a function of temperature calculated by (i) phonon plus thermal electronic contribution, (ii) Debye–Grüneisen model (high temperature and low temperature cases) plus thermal electronic contribution, and (iii) Debye–Wang model ($\lambda = 0$, ±0.5, and ±1) plus thermal electronic contribution. The measured values (open cycles) are also shown for Ni [39] and Ni$_3$Al [40].
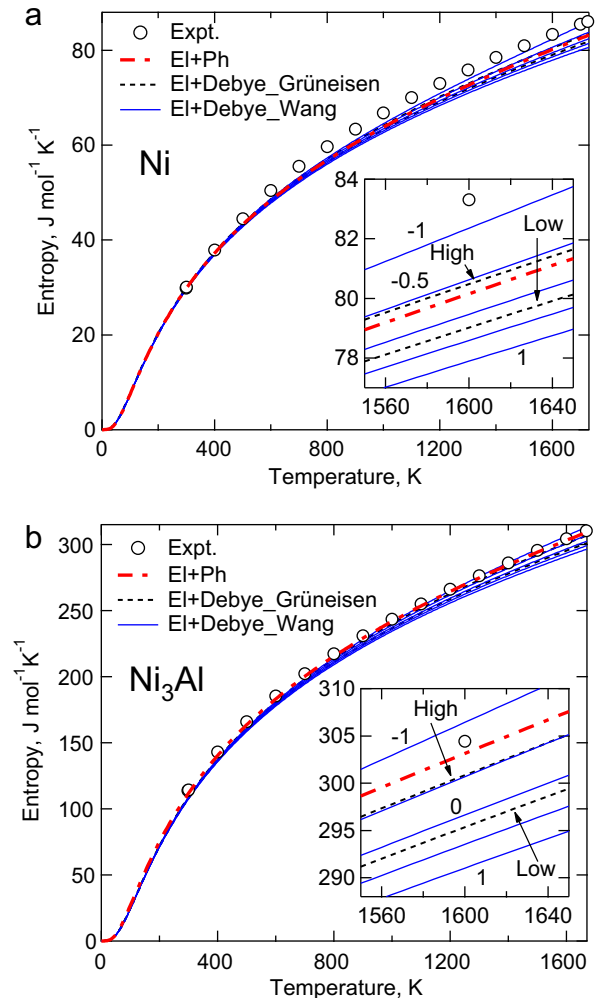


Fig. 6. Entropies for Ni and Ni$_3$Al as a function of temperature calculated by (i) phonon plus thermal electronic contribution, (ii) Debye–Grüneisen model (high temperature and low temperature cases) plus thermal electronic contribution, and (iii) Debye–Wang model ($\lambda = 0$, ±0.5, and ±1) plus thermal electronic contribution. Note that the unit for Ni is per mole atom, and for Ni$_3$Al it is per mole formula with four atoms. The recommended values (open cycles) are also shown for Ni and Ni$_3$Al [44].

Fig. 6 illustrates the entropies of Ni and Ni$_3$Al calculated by phonon, Debye–Grüneisen model, Debye–Wang model, where the entropy is obtained by $S = -(\partial F/\partial T)_V$ under $P = 0$. The recommended entropies [44] are also shown in Fig. 6 for comparison, which are slightly higher than the phonon results, especially for Ni in the intermediate temperature range. Regarding the Debye model, the predictions from the high temperature case of Debye–Grüneisen model and $\lambda = -1$ of Debye–Wang model agree with the recommended values.

Fig. 7 shows the enthalpies of Ni and Ni$_3$Al obtained by phonon, Debye–Grüneisen model, Debye–Wang model, together with the recommended values [44], where the enthalpy at $P = 0$ is obtained by $H = F + TS$ and the reference state is the commonly used setting in CALPHAD community [45], i.e. the $H$ at 298.15 K and 1 bar. Note that the enthalpy and internal energy are equal at $P = 0$. Fig. 7 shows that the phonon predictions agree well with the recommended values of Ni$_3$Al, and slightly larger than the recommended ones of Ni. For Debye model, the results from the high temperature case of Debye–Grüneisen model and $\lambda = -0.5$ of Debye–Wang model agree with the recommended values and also the phonon results.
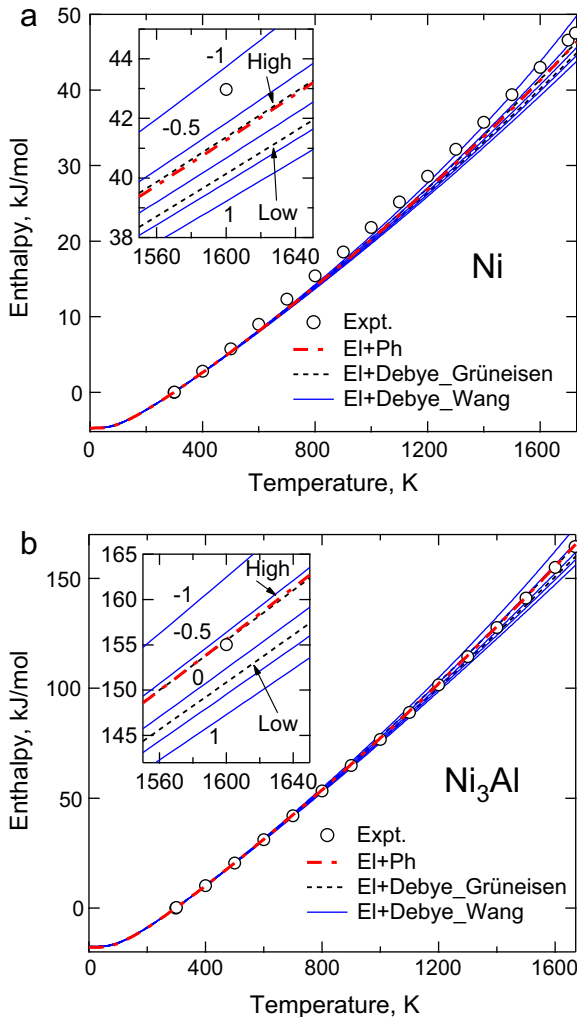
In the present work, heat capacity at constant pressure is estimated by,

$$C_P = C_V + \beta^2 BTV \tag{22}$$

where $C_V$ is the heat capacity at constant volume estimated by $C_V = T(\partial S/\partial T)_V$. $\beta$ is the volume thermal expansion coefficient which is three times larger than the linear one given by Eq. (21), i.e., $\beta = 3\alpha$. The $B$, $T$, and $V$ are the bulk modulus, temperature and volume, respectively. Using the results of linear thermal expansion coefficients in Fig. 4, the bulk moduli in Fig. 5, and the estimated $C_V$, the results of $C_P$ at $P = 0$ are plotted in Fig. 8 based on phonon, Debye–Grüneisen model, and Debye–Wang model. The recommended values of Ni [42] and Ni$_3$Al [44] are also shown in Fig. 8. It is found that the phonon results are in good agreement with the recommended values, especially for Ni. For Debye model, the results from the high temperature case of Debye–Grüneisen model and $\lambda = 0$ of Debye–Wang model describe well the recommended values.

By considering all the thermodynamic properties of Ni and Ni$_3$Al predicted herein, including thermal expansion coefficient, bulk modulus, entropy, enthalpy and heat capacity, we find that (i) the phonon plus thermal electronic contributions describe well
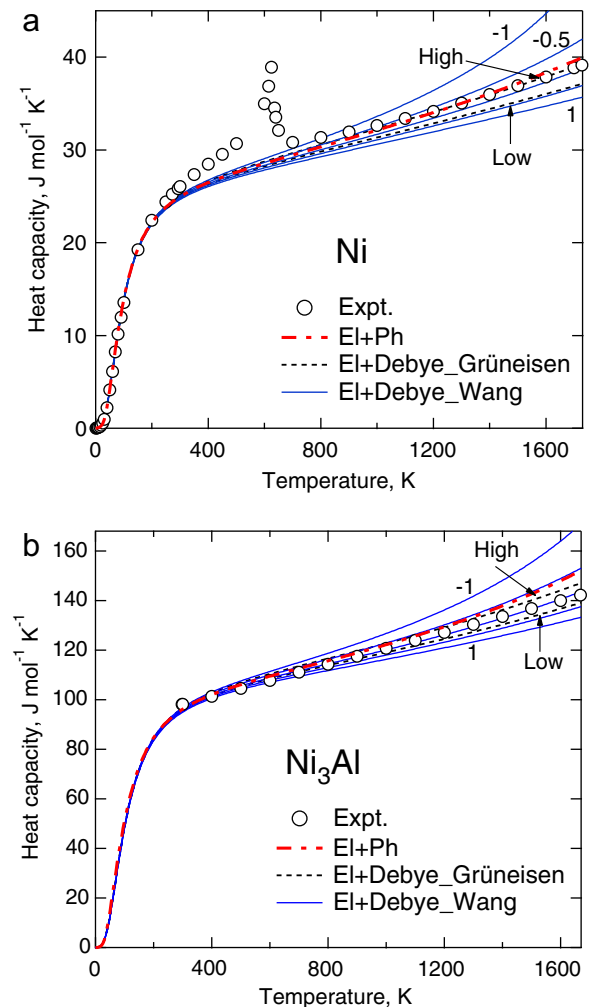


Fig. 7. Enthalpies for Ni and Ni$_3$Al as a function of temperature calculated by (i) phonon plus thermal electronic contribution, (ii) Debye–Grüneisen model (high temperature and low temperature cases) plus thermal electronic contribution, and (iii) Debye–Wang model ($\lambda = 0, \pm0.5,$ and $\pm1$) plus thermal electronic contribution. The recommended values (open cycles) are also shown for Ni and Ni$_3$Al [44]. Note that the unit for Ni is per mole atom, and for Ni$_3$Al it is per mole formula with four atoms.



Fig. 8. Heat capacities for Ni and Ni$_3$Al as a function of temperature calculated by (i) phonon plus thermal electronic contribution, (ii) Debye–Grüneisen model (high temperature and low temperature cases) plus thermal electronic contribution, and (iii) Debye–Wang model ($\lambda = 0, \pm0.5,$ and $\pm1$) plus thermal electronic contribution. The recommended values (open cycles) are also shown for Ni [42] and Ni$_3$Al [44]. Note that the unit for Ni is per mole atom, and for Ni$_3$Al it is per mole formula with four atoms.

the thermodynamics except for the bulk modulus and (ii) the results from the high temperature case of Debye–Grüneisen model and $\lambda = -0.5$ of Debye–Wang model (thermal electronic contribution included in Debye model) are comparable with the phonon results and also the experiments.

## 5. Conclusions

Temperature-dependent thermodynamic properties of Ni and Ni$_3$Al, including thermal expansion coefficient, bulk modulus, entropy, enthalpy and heat capacity, have been studied in terms of first-principles calculations and quasiharmonic approach, wherein the thermal electronic and vibrational contributions are considered. Nine energy vs. volume ($E$–$V$) equations of state (EOS's) are presented in detail and fitted to the first-principles calculated $E$–$V$ points. It is found that the 4-parameter Birch-Murnaghan EOS gives a good account for both Ni and Ni$_3$Al, while the Murnaghan EOS and the logarithmic EOS are the worse ones among the 4-parameter EOS's. At finite temperatures, comparative studies are performed between phonon, Debye–Grüneisen and Debye–Wang models, it is found that the thermodynamic properties of Ni and Ni$_3$Al studied herein (except for the bulk modulus) are described well by phonon and thermal electronic contributions, and also by Debye model through choosing suitable parameters, i.e., the high temperature case of Debye–Grüneisen model and $\lambda = -0.5$ of Debye–Wang model. The presently comparative studies of Ni and Ni$_3$Al between phonon and Debye model, as well as by different EOS's, provide helpful insights into the study of thermodynamics of solid phases.

## Appendix A

For BM4 EOS, i.e., Eq. (2) with $n = 2$ and $e = 0$, the equilibrium properties $V_0$, $B_0$, and $B_0'$ can be estimated by the following equations:

$$V_0 = \sqrt{\frac{9bcd - 4c^3 - \sqrt{(c^2 - 3bd)(4c^2 - 3bd)^2}}{b^3}} \tag{A1}$$

$$B_0 = \frac{2(27d + 14cV_0^{2/3} + 5bV_0^{4/3})}{9V_0^3} \tag{A2}$$

**Table A1**
Fitting parameters $a$, $b$, $c$, $d$, and $e$ represented by equilibrium properties $E_0$, $V_0$, $B_0$, $B_0'$, and $B_0''$ for BM4, BM5, mBM4, mBM5, LOG4, LOG5 and Morse EOS's.

| EOS | Equation |
|---|---|
| BM4 | $a = E_0 + 9B_0V_0(6 - B_0')/16$ |
| | $b = -9B_0V_0^{5/3}(16 - 3B_0')/16$ |
| | $c = 9B_0V_0^{7/3}(14 - 3B_0')/16$ |
| | $d = -9B_0V_0^3(4 - B_0')/16$ |
| BM5 | $a = E_0 + 3B_0V_0(287 + 9B_0B_0'' - 87B_0' + 9B_0'^2)/128$ |
| | $b = -3B_0V_0^{5/3}(239 + 9B_0B_0'' - 81B_0' + 9B_0'^2)/32$ |
| | $c = 9B_0V_0^{7/3}(199 + 9B_0B_0'' - 75B_0' + 9B_0'^2)/64$ |
| | $d = -3B_0V_0^3(167 + 9B_0B_0'' - 69B_0' + 9B_0'^2)/32$ |
| | $e = 3B_0V_0^{11/3}(143 + 9B_0B_0'' - 63B_0' + 9B_0'^2)/128$ |
| mBM4 | $a = E_0 + 9B_0V_0(4 - B_0')/2$ |
| | $b = -9B_0V_0^{4/3}(11 - 3B_0')/2$ |
| | $c = 9B_0V_0^{5/3}(10 - 3B_0')/2$ |
| | $d = -9B_0V_0^2(3 - B_0')/2$ |
| mBM5 | $a = E_0 + 3B_0V_0(122 + 9B_0B_0'' - 57B_0' + 9B_0'^2)/8$ |
| | $b = -3B_0V_0^{4/3}(107 + 9B_0B_0'' - 54B_0' + 9B_0'^2)/2$ |
| | $c = 9B_0V_0^{5/3}(94 + 9B_0B_0'' - 51B_0' + 9B_0'^2)/4$ |
| | $d = -3B_0V_0^2(83 + 9B_0B_0'' - 48B_0' + 9B_0'^2)/2$ |
| | $e = 3B_0V_0^{7/3}(74 + 9B_0B_0'' - 45B_0' + 9B_0'^2)/8$ |
| LOG4 | $a = E_0 + B_0V_0[3(\ln V_0)^2 + (B_0' - 2)(\ln V_0)^3]/6$ |
| | $b = -B_0V_0[2\ln V_0 + (B_0' - 2)(\ln V_0)^2]/2$ |
| | $c = B_0V_0[1 + (B_0' - 2)\ln V_0]/2$ |
| | $d = -B_0V_0(B_0' - 2)/6$ |
| LOG5 | $a = E_0 + B_0V_0[12(\ln V_0)^2 + 4(B_0' - 2)(\ln V_0)^3 + (3 + B_0B_0'' - 3B_0' + B_0'^2)(\ln V_0)^4]/24$ |
| | $b = -B_0V_0[6\ln V_0 + 3(B_0' - 2)(\ln V_0)^2 + (3 + B_0B_0'' - 3B_0' + B_0'^2)(\ln V_0)^3]/6$ |
| | $c = B_0V_0[2 + 2(B_0' - 2)\ln V_0 + (3 + B_0B_0'' - 3B_0' + B_0'^2)(\ln V_0)^2]/4$ |
| | $d = -B_0V_0[-2 + B_0' + (3 + B_0B_0'' - 3B_0' + B_0'^2)\ln V_0]/6$ |
| | $e = B_0V_0(3 + B_0B_0'' - 3B_0' + B_0'^2)/24$ |
| Morse | $a = E_0 + 9B_0V_0(B_0' - 1)^{-2}/2$ |
| | $b = -9B_0V_0(B_0' - 1)^{-2}\exp(B_0' - 1)$ |
| | $c = 9B_0V_0(B_0' - 1)^{-2}\exp(2B_0' - 2)/2$ |
| | $d = (1 - B_0')V_0^{-1/3}$ |

$$B'_0 = \frac{243d + 98cV_0^{2/3} + 25bV_0^{4/3}}{81d + 42cV_0^{2/3} + 15bV_0^{4/3}} \tag{A3}$$

See Table A1.

## References

[1] Y. Wang, Z.K. Liu, L.Q. Chen, Acta Mater. 52 (2004) 2665–2671.
[2] R. Arroyave, D. Shin, Z.K. Liu, Acta Mater. 53 (2005) 1809–1819.
[3] R. Arroyave, Z.K. Liu, Phys. Rev. B 74 (2006) 174118.
[4] T. Mohri, Y. Chen, J. Alloy Compd. 383 (2004) 23–31.
[5] V.L. Moruzzi, J.F. Janak, K. Schwarz, Phys. Rev. B 37 (1988) 790–799.
[6] F. Peng, H.Z. Fu, X.D. Yang, Solid State Commun. 145 (2008) 91–94.
[7] S. Shang, A.J. Böttger, Acta Mater. 53 (2005) 255–264.
[8] S.L. Shang, Y. Wang, Z.K. Liu, Phys. Rev. B 75 (2007) 024302.
[9] L. Vocadlo, J.P. Poirer, G.D. Price, Am. Mineral. 85 (2000) 390–395.
[10] A.R. Oganov, J.P. Brodholt, G.D. Price, Phys. Earth Planet Inter. 122 (2000) 277–288.
[11] V. Deodeshmukh, N. Mu, B. Li, B. Gleeson, Surf. Coat. Technol. 201 (2006) 3836–3840.
[12] B. Gleeson, J. Propul. Power 22 (2006) 375–383.
[13] S. Baroni, S. de Gironcoli, A. Dal Corso, P. Giannozzi, Rev. Mod. Phys. 73 (2001) 515–562.
[14] A. van de Walle, G. Ceder, Rev. Mod. Phys. 74 (2002) 11–45.
[15] G. Kresse, J. Furthmuller, Comp. Mater. Sci. 6 (1996) 15–50.
[16] G. Kresse, J. Furthmuller, Phys. Rev. B 54 (1996) 11169–11186.
[17] A. van de Walle, M. Asta, G. Ceder, Calphad 26 (2002) 539–553.
[18] F. Birch, Phys. Rev. 71 (1947) 809–824.
[19] F. Birch, J. Geophys. Res. 83 (1978) 1257–1268.
[20] D.M. Teter, G.V. Gibbs, M.B. Boisen, D.C. Allan, M.P. Teter, Phys. Rev. B 52 (1995) 8064–8073.
[21] J.P. Poirier, A. Tarantola, Phys. Earth Planet Inter. 109 (1998) 1–8.
[22] F.D. Murnaghan, Am. J. Math. 59 (1937) 235–260.
[23] P. Vinet, J. Ferrante, J.R. Smith, J.H. Rose, J. Phys, C. Solid, State 19 (1986) L467–L473.
[24] P. Vinet, J.R. Smith, J. Ferrante, J.H. Rose, Phys. Rev. B 35 (1987) 1945–1953.
[25] K.H. Hellwege, J.L. Olsen, Phonon States of Elements, Electron States and Fermi Surfaces of Alloys, vol. 13, Springer, Berlin, 1981. p. 17.
[26] O.L. Anderson, Equations of State of Solids for Geophysics and Ceramic Science, Oxford university press, New York, 1995.
[27] H.C. Herper, E. Hoffmann, P. Entel, Phys. Rev. B 60 (1999) 3839–3848.
[28] Y. Wang, R. Ahuja, B. Johansson, Int. J. Quantum Chem. 96 (2004) 501–506.
[29] X.G. Lu, M. Selleby, B. Sundman, Acta Mater. 53 (2005) 2259–2272.
[30] X.G. Lu, M. Selleby, B. Sundman, Acta Mater. 55 (2007) 1215–1226.
[31] P.E. Blöchl, Phys. Rev. B 50 (1994) 17953–17979.
[32] G. Kresse, D. Joubert, Phys. Rev. B 59 (1999) 1758–1775.
[33] J.P. Perdew, K. Burke, M. Ernzerhof, Phys. Rev. Lett. 77 (1996) 3865–3868.
[34] S. Shang, A.J. Böttger, M.P. Steenvoorden, M.W.J. Craje, Acta Mater. 54 (2006) 2407–2417.
[35] H.J. Monkhorst, J.D. Pack, Phys. Rev. B 13 (1976) 5188–5192.
[36] P.E. Blöchl, O. Jepsen, O.K. Andersen, Phys. Rev. B 49 (1994) 16223–16233.
[37] M. Methfessel, A.T. Paxton, Phys. Rev. B 40 (1989) 3616–3621.
[38] P. Villars, L.D. Calvert, Pearson's Handbook of Crystallographic Data for Intermetallic Phases, ASTM International, Newbury, OH, 1991.
[39] G. Simmons, H. Wang, Single Crystal Elastic Constants and Calculated Aggregate Properties: A Handbook, MIT Press, Cambridge, 1971.
[40] S.V. Prikhodko, J.D. Carnes, D.G. Isaak, H. Yang, A.J. Ardell, Metall. Mater. Trans. A 30 (1999) 2403–2408.
[41] C. Stassis, F.X. Kayser, C.K. Loong, D. Arch, Phys. Rev. B 24 (1981) 3048–3053.
[42] Y.S. Touloukian, C.Y. Ho, Properties of Selected Ferrous Alloying Elements, Hemisphere Publishing Corporation, New York, 1989.
[43] Y.S. Touloukian, Thermophysical Properties of Matter: The TPRC Data Series, Thermal Expansion: Metallic Elements and Alloys, vol. 12, Plenum, New York, 1975.
[44] I. Barin, Thermochemical Data of Pure Substances, Weinheim, New York, 1995.
[45] N. Saunders, A.P. Miodownik, CALPHAD (Calculation of Phase Diagrams): A Comprehensive Guide, Pergamon, Oxford, New York, 1998.